file s020_sys_k3.tex, Kirk McDonald, Aug. 12, 2006
Comments in sans serif
Modifications in slanted type
Original text in Roman

1. I recommend that we switch to the Standard European convention of putting a space between a citation and the preceding word. Thus, CHOOZ experiment [7] rather than CHOOZ experiment[7]. This change requires tinkering with some LaTeX setup file, so I have not been able to enforce it myself. I have put spaces in front of citations, but they don't appear in the output, in general.

2. Looking at[7],
http://puhep1.princeton.edu/~mcdonald/examples/neutrinos/apollonio_epj_c27_331_03.pdf
we see the convention refered to in comment 1, and we see that they spell it CHOOZ and not Chooz.

3. I notice that the typography of the references does not quite follow the conventions recommended in db-latex.tex. I have changed the references to do so. While these changes are mostly invisible, experts can detect them. Also, a few bad references have been fixed....

4. I have put the hyphen in compount adjectives, as beloved by Phys. Rev. editors.

5. We should never write "errors" in a formal document, only "uncertainties"!!!! (We should also speak this way, but I know that won't happen.

6. Ref 6dchooz has been updated to point to a very recent document. I added Vogel's paper to ref 7illbeta.

7. The big issue is that there seems to me to be a large gap in the structure of chaps 1-3. Namely, we don't introduce the concept/principle of our measurement anywhere. Chap 1 talks about physics – that we can an should measure $\sin^2 2\theta_{13}$. Chap 2 jumps in to talk about uncertainties on a measurement that has never been defined. Chap 3 talks about the equipment needed to make the measurement – without quite saying what the measurement is. So, I'm making an attempt at writing what seems to me to be the missing section. I will place it as sec. 2.1. However, it could be be that we should swap chaps. 2 and 3 (and use the new section as sec. 2.1 of the chapter on the experimental overview). It could that the new section should be used to enlarge sec. 1.4.

2 *Principle of the Measurement of* $\sin^2 2\theta_{13}$**, Sensitivity & Systematic** *Uncertainties*

2.1 Principle of the Measurement of $\sin^2 2\theta_{13}$

The Daya Bay Reactor Neutrino Experiment will measure the disappeance of electron antineutrinos ($\bar{\nu}_e$) as a function of distance from their production in the Daya Bay reactor complex. As discussed in sec. 1.3.1, the probability that an antineutrino that is created as a $\bar{\nu}_e$ of energy E remains a $\bar{\nu}_e$ after traveling a distance L can be written as

$$P_{\rm sur} = 1 - P_{\rm dis} \approx 1 - A(E, L) \sin^2 2\theta_{13}, \tag{1}$$

where the "analyzing power" A for $E \approx 1$-10 MeV and $L < 2$ km has the form

$$A(E, L) = \sin^2 \Delta_{31} = \sin^2 \left[1,267 \Delta m^2_{31} (\mathrm{eV}/c^2)^2 \frac{L(\mathrm{km})}{E(\mathrm{MeV})}\right] \approx \sin^2 \left[2.8 \frac{L(\mathrm{km})}{E(\mathrm{MeV})}\right], \tag{2}$$

using the current best estimate[29] that the neutrino mass splitting parameter Δm^2_{31} is 2.2 ± 0.5 (eV/c^2)^2.

2.1.1 One detector, one reactor, one distance

If a single neutrino detector is placed at a distance L from a single nuclear reactor, the number $N(E)$ of detected neutrino interactions in an interval dE about energy E during time t can be written as the product

$$N(E) = \frac{\phi_r(E, dE, t)}{L^2_{rd}} p_{\bar{\nu}} M_d \epsilon_d (1 - A \sin^2 2\theta_{13}) \equiv \frac{\phi_r K}{L^2_{rd}} (1 - A \sin^2 2\theta_{13}) \tag{3}$$

where $\phi_r(E, dE, t)$ is the total flux at unit distance of antineutrinos from the reactor during time t in interval dE about E, L_{rd} is the distance from the reactor to the detector, $p_{\bar{\nu}_e}$ is the probability of a neutrino interaction $\bar{\nu}_e + p \rightarrow n + e^+$ per unit detector mass, M_d is the detector mass, ϵ_d is the detection efficiency, and $K = p_{\bar{\nu}_e} M_d \epsilon_d$.

The spectrum of reactor antineutrinos falls with energy, while the cross section for rises with energy. As shown in Fig. 2.1 the most probable energy for observation of inverse β decay is for an antineutrino energy of 4 MeV.

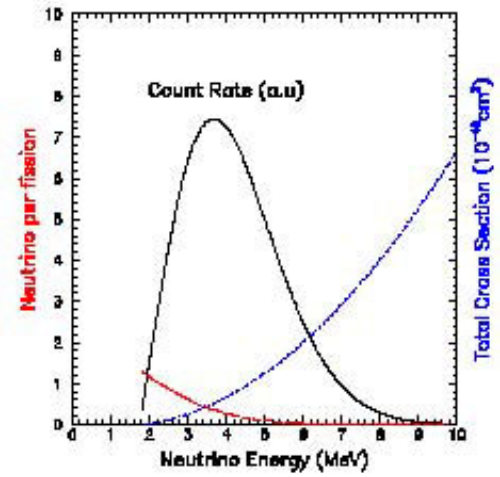

Fig. 2.1. The $\bar{\nu}_e$ production rate in a nuclear reactor, the cross section for inverse β decay, and the probability of observation of the inverse $beta$ decay process in a reactor neutrino experiment, as a function of the energy of the antineutrino. I "stole" this figure from the V3.3 proposal. Can we get a better copy? Should we add a reference here?

Clearly, the distance L_{rd} should be chosen such that the analying power A is maximal. Using $\Delta m^2_{31} = 2.2$ (eV/c^2)^2 in eq. (2), the analyzing power would be 1 for $L = 2.25$ km and $E = 4$ MeV.

In principle, a determination of $\sin^2 2\theta_{13}$ can be made using eq.(3) using a single detector at a single distance from a single reactor. The distance L can be well measured, the neutrino flux ϕ can be calculated reasonably well from measurement of the reactor power[27], but the factor K is not well known in practice. Hence, extensions of the measurement technique are desirable that reduce the dependence of the result for $\sin^2 2\theta_{13}$ on the product ϕK.

2.1.2 One detector, one reactor, two distances

If a single detector is operated at different times at two distances L_1 and L_2 from a single reactor, two sets of neutrino interactions N_1 and N_2 can be observed. The ratio of these observations is

$$\frac{N_2}{N_1} = \frac{1 - A(L_2)\sin^2 2\theta_{13}}{1 - A(L_1)\sin^2 2\theta_{13}}\,, \tag{4}$$

assuming that the factors ϕ_r and K are independent of time.

To minimize the time of the experiment, L_1 should be much less than L_2. Then if $A(L_2) \approx 1$ we have $A(L_1) \approx 0$ and

$$\frac{N_2}{N_1} \approx 1 - \sin^2 2\theta_{13}, \qquad \sin^2 2\theta_{13} \approx 1 - \frac{N_2}{N_1}\,. \tag{5}$$

Thus, the use of two distances, usually called "near" and "far", largely eliminates the dependence of the measurement of $\sin^2 2\theta_{13}$ on the imperfectly known quantities ϕ_r and K.

Note that from the two measurements, N_1 and N_2, the unknown product $\phi_r K$ is determined as well as $\sin^2 2\theta_{13}$.

2.1.3 Two detectors, one reactor, two distances

One way to improve the statistical accuracy of the measurement of $\sin^2 2\theta_{13}$ in a fixed time is by use of multiple detectors.

For example, if N_{ij} is the the number of antineutrino interactions observed in detector i when at distance L_j from the reactor, then

$$N_{i,j} = \frac{\phi_r K_i}{L_j^2}(1 - A(L_j)\sin^2 2\theta_{13}). \tag{6}$$

The value of the constant K_i could well be different for different detectors. To minimize the effect of the possible variation of the constant K_i between detectors, they should not be operated at a single distance. Rather, each detector should be operated in turn at both distances L_1 and L_2, which requires "swapping" the two detectors at the midpoint of the duraction of the experiment. Then, if $A(L_1) \approx 0$ and $A(L_2) \approx 1$, we measure

$$\sin^2 2\theta_{13} \approx 2 - \frac{N_{1,2}}{N_{1,1}} - \frac{N_{2,2}}{N_{2,1}}\,. \tag{7}$$

Note that the four measurements $N_{i,j}$ suffice to determine the four unknown quantities $\sin^2 2\theta_{13}$, ϕ_r, K_1 and K_2.

2.1.4 8 detectors, 6 reactors (the Daya Bay Reactor Neutrino Experiment)

Nuclear reactor complexes typically have more than one reactor. If we observe antineutrino interactions from m reactors with a set of n detectors, there are $m + n + 1$ unknowns, $\sin^2 2\theta_{13}$, The reactor fluxes ϕ_j for $j = 1$ to m, and the detector constants K_i for $i = 1$ to n.

A single configuration of the detectors around the reactors leads to the observation of n numbers of events in the n detectors. If k different configurations are the detectors are used over the course of the experiment, a total of kn measurements are made. If $\sin^2 2\theta_{13}$ is to be determined with no dependence on the $m + n$ fluxes and detector constants, then kn must be greater than or equal to $m + n + 1$.

The Daya Bay reactor complex will have $m = 6$ reactors operational by the completion of the experiment. To determine $\sin^2 2\theta_{13}$ independent of the K_i and the ϕ_j with only two detector configurations requires a minimum of $n = 7$ detectors.

The proposal is to use 8 detectors, arrayed in two "near" groups of two detectors, and one "far" group of 4 detectors, as shown in Fig. 2.2.

Fig. 2.2. Layout of the Daya Bay *reactor neutrino* experiment.

To a first approximation, the analyzing powers (2) are unity for detectors and the far site, and zero for detectors at the near sites.

We consider two configurations, indicated by superscripts $^{(1)}$ and $^{(2)}$, that in configuration 1 detectors 1-4 are at near sites while detectors 5-8 are at the far site. Then, in configuration 2 detectors 1-4 are at the far site and detectors 5-8 are at near far sites.

The observed rates $N_i^{(k)}$ of antineutrino events in the 8 detectors can be written as

$$N_i^{(1)} = K_i \sum_{j=1}^{6} \frac{\phi_j}{(L_{i,j}^{(1)})^2}, \qquad i = 1\text{-}4, \tag{8}$$

$$N_i^{(1)} = K_i \sum_{j=1}^{6} \frac{\phi_j}{(L_{i,j}^{(1)})^2}(1 - \sin^2 2\theta_{13}), \qquad i = 5\text{-}8, \tag{9}$$

$$N_i^{(2)} = K_i \sum_{j=1}^{6} \frac{\phi_j}{(L_{i,j}^{(2)})^2}(1 - \sin^2 2\theta_{13}), \qquad i = 1\text{-}4, \tag{10}$$

$$N_i^{(2)} = K_i \sum_{j=1}^{6} \frac{\phi_j}{(L_{i,j}^{(2)})^2}, \qquad i = 5\text{-}8, \tag{11}$$

We form the 8 ratios,

$$\frac{N_i^{(2)}}{N_i^{(1)}} = \frac{\sum_{j=1}^{6} \frac{\phi_j}{(L_{i,j}^{(2)})^2}}{\sum_{j=1}^{6} \frac{\phi_j}{(L_{i,j}^{(1)})^2}}(1 - \sin^2 2\theta_{13}) = \rho(1 - \sin^2 2\theta_{13}) \qquad i = 1\text{-}4, \tag{12}$$

$$\frac{N_i^{(1)}}{N_i^{(2)}} = \frac{\sum_{j=1}^{6} \frac{\phi_j}{(L_{i,j}^{(1)})^2}}{\sum_{j=1}^{6} \frac{\phi_j}{(L_{i,j}^{(2)})^2}}(1-\sin^2 2\theta_{13}) = \frac{1}{\rho}(1-\sin^2 2\theta_{13}) \qquad i = \textit{5-8}, \tag{13}$$

where

$$\rho = \frac{\sum_{j=1}^{6} \frac{\phi_j}{(L_{i,j}^{(2)})^2}}{\sum_{j=1}^{6} \frac{\phi_j}{(L_{i,j}^{(1)})^2}} \tag{14}$$

is the ratio of the sums of the reactor fluxes weighted by distance in the two configurations of the experiment.

Our measurement of $\sin^2 2\theta_{13}$ *is then*

$$\sin^2 2\theta_{13} = 8 - \rho \sum_{i=1}^{4} \frac{N_i^{(2)}}{N_i^{(1)}} - \frac{1}{\rho} \sum_{i=5}^{8} \frac{N_i^{(1)}}{N_i^{(2)}} \,. \tag{15}$$

Equation (15) is a generalization of eqs. (5) and (7), and likewise involves ratios of rates in "far" detectors to those in "near" detectors. The detector factors K_i *do not appear in eq. (15), but ratios of the reactor fluxes* ϕ_j *do appear.*

2.2 *Needs a name*

The control of systematic *uncertainties* is critical to achieving the $\sin^2 2\theta_{13}$ sensitivity goal of this experiment. The most relevant previous experience is the *CHOOZ* experiment[7] which obtained $\sin^2 2\theta_{13} < 0.17$ for $\Delta m^2_{31} = 2.5 \times 10^{-3}\text{eV}^2$ at 90% *confidence level* don't use undefined abbreviations such as "C.L.", the best limit to date, with a systematic uncertainty of 2.7% and statistical uncertainty of 2.8%. In order to achieve a $\sin^2 2\theta_{13}$ sensitivity below 0.01, both the statistical and systematic uncertainties need to be an order of magnitude smaller than CHOOZ. The projected statistical *uncertainty* of the Daya Bay far detectors is 0.2% with three years data taking. In this section we discuss our strategy for achieving the level of systematic *uncertainty* comparable to that of the statistical *uncertainty*. Achieving this very ambitious goal will require extreme care and substantial effort that can only be realized by incorporating rigid constraints in the design of the experiment.

There are three main sources of systematic uncertainties: reactor, background, and detector. Each source of *uncertainty* can be further classified into correlated and uncorrelated *uncertainties*.

2.3 *Reactor-related uncertainties*

For a reactor plant with only one core, all *uncertainties* from the reactor, correlated or uncorrelated, can be canceled precisely by using one far detector and one near detector (assuming the average distances are precisely known)[22]. In reality, the Daya Bay Power Plant has four cores in two groups, the Daya Bay Plant and the Ling Ao Plant. Another two cores will be installed adjacent to Ling Ao, called Ling Ao II, which will start to generate electricity in 2010. Fig. 2.2 shows the locations of the Daya Bay cores, Ling Ao cores, and the future Ling Ao II cores. Superimposed on the figure are the tunnelling scheme and the proposed detector sites. The distance between the two cores at each reactor site, called a pair here, is about 88 m. The Daya Bay pair is 1100 m from the Ling Ao pair, and the maximum span of cores will reach 1600 m when Ling Ao II starts operation.

Reactor systematic *uncertainties* are associated with leave out "uncertainties in" the power levels of the different cores and the effective locations of the cores relative to the detectors.

2.3.1 Power fluctuations

Typically, the measured power level for each reactor core will have a correlated (common to all the reactors) *uncertainty* of the order of 2% and an uncorrelated *uncertainty* of similar size. Optimistically, we may be able to achieve uncorrelated *uncertainties* of 1%, but we conservatively assume that each reactor has

2% uncorrelated *uncertainty* in the following. If the distances are precisely known, the correlated uncertainties will cancel in the near/far ratio. In the multiple-reactor (> 2) case one cannot separately measure the event rate from each reactor. We will measure the following combination of ratios in the event rates of the far and near detectors:

$$\rho = \left[\alpha \sum_r \frac{\phi_r}{(L_r^{DB})^2} + \sum_r \frac{\phi_r}{(L_r^{LA})^2} \right] \Big/ \sum_r \frac{\phi_r}{L_{rf}^2} \tag{16}$$

where ϕ_r is the antineutrino flux at unit distance from core r, L_{rf} is the distance from reactor r to the far site, L_r^{DB} (L_r^{LA}) is the distance from reactor r to the near Daya Bay (Ling Ao) site, and α is a constant chosen to minimize the sensitivity of ρ to the relative reactor power levels. The optimal choice of $\alpha \neq 1$ will substantially reduce the systematic *uncertainty* associated with uncorrelated reactor power levels while introducing a slight increase in the statistical *uncertainty*. The correlated *uncertainties* of the reactors are common to both the numerator and denominator of the ratio ρ, and therefore will be cancelled.

We assume a detector configuration shown in Fig. 2.2, with two near sites at ~ 500 m baselines to sample the reactor cores and the far site at an average baseline of ~ 1800 m. For an uncorrelated *uncertainty* of 2% for each core and optimal choice of α, Table 2.1 shows the estimated reactor power contribution to σ_ρ (*i.e.*, the *uncertainty* in the ratio combination ρ) for the two cases of 4 reactor cores and 6 reactor cores.

2.3.2 Location uncertainties

The location of the reactor cores will be determined to a precision of about 30 cm. We assume that the location *uncertainties* are uncorrelated, and so their combined effect will be reduced by $\sim \sqrt{N_r}$ where N_r is the number of reactor cores. The resulting *uncertainty* in the far/near event ratio is estimated to be 0.08% for the near baseline of ~ 500 m.

Number of cores	σ_ρ(power)	σ_ρ(location)	σ_ρ(total)
4	0.035%	0.08%	0.087%
6	0.097%	0.08%	0.126%

Table 2.1. Reactor-related systematic *uncertainties* for different reactor configurations. The uncorrelated *uncertainty* of a single core is assumed to be 2%.

2.3.3 *Spent-fuel uncertainties*

2.4 *Detector-related uncertainties*

For the detector-related *uncertainties*, we consider the CHOOZ results as a reference, and then compute 2 values for the Daya Bay case: baseline and goal. The baseline value is that we expect to be achievable through essentially proven methods with perhaps straightforward improvement in technique and accounting for the fact that we need to consider only *relative uncertainties* between near and far detectors. The goal value is that which we consider reachable through improved methods and extra care beyond the level of previous experiments of this type. The results are summarized in Table 2.2 and discussed in the rest of this section.

2.4.1 Target mass and H/C ratio

The antineutrino targets are the free protons in the detector, so the event rate in the detector is proportional to the total mass of free protons. The systematic *uncertainty* in this quantity is controlled by precise knowledge of the relative total mass of the central volumes of the detector modules as well as filling the modules from a common batch of scintillator liquid so that the H/C ratio is the same to high precision.

The mass of the central detector is accurately determined in several ways. First the detector modules will be built to specified tolerance so that the volume is known to $\sim 0.1\%$ (typically $<$1 mm dimension

Source of *uncertainty*		CHOOZ	Daya Bay	
			Baseline	Goal
# protons	H/C ratio	0.8	0.2	0.1
	Mass	-	0.2	0.02
Detector Efficiency	Energy cuts	0.8	0.2	0.05
	Position cuts	0.32	0.0	0.0
	Time cuts	0.4	0.1	0.03
	H/Gd ratio	1.0	0.1	0.1
	n multiplicity	0.5	0.05	0.01
	Trigger	0	0.01	0.01
	Live time	0	< 0.01	< 0.01
Total detector-related uncertainty		1.7%	0.38%	0.15%

Table 2.2. Comparison of detector-related systematic uncertainties (all in percent, per detector module) of CHOOZ experiment and projections for Daya Bay. Baseline values for Daya Bay are achievable through essentially proven methods, whereas the goals should be attainable through additional efforts described in the text.

out of several meters). We will make measurements of these volumes after construction to characterize them to higher precision than 0.1%. We plan to fill each module from a common stainless steel tank at a controlled constant temperature. We will measure the fluid flow using premium grade precision flowmeters with a repeatability specification of 0.02%. Several flowmeters will be run in series for redundancy. Residual topping up of the detector module to a specified level (only about ~ 20 kg since the volume is known and measured) is measured with the flowmeters as well. We aim for a goal of 0.02% relative precision on the central detector mass based on the specification of the flowmeters. We quote a baseline of 0.2%, which should be fairly straightforward even if we rely on the absolute calibration of flowmeters alone.

The absolute H/C ratio was determined by CHOOZ using scintillator combustion and analysis to 0.8% precision based on several laboratories. We will only require that the *relative* measurement on different samples be known, so an improved precision of 0.2% or better is expected.

We are presently engaged in a program of R&D with the goal of measuring the *relative* H/C ratio in different samples of liquid scintillator to $\sim 0.1\%$ precision. We are exploring two different methods the achieve this goal: precision NMR and neutron capture. The neutron capture method would need to be utilized before the introduction of Gd into the scintillator, but could be used to precisely characterize the organic liquids used in the liquid scintillator cocktail. In principle, the NMR method could be used on the final Gd-loaded scintillator.

In addition, we will need to determine the *relative* H/C ratio in the gamma catcher liquid scintillator to about 1%. This is to control the relative amount of "spill-in" events where a neutron generated in the gamma catcher is captured in the Gd-loaded scintillator after thermal diffusion. Differences in spill-in and spill-out fractions between different detector modules must be understood, and the H/C ratio in the gamma catcher must be determined to 1% to insure that we can achieve the baseline systematic *uncertainty* in Table 2.2.

As discussed in 2.5.1 below, we intend to deploy the detector modules in designated pairs. For each of the 4 pairs, one detector will be at a near site and one at a far site. We plan to fill the detector module pairs simultaneously from the same batch of scintillator (for Gd-loaded and gamma-catcher as well). Thus each pair should have identical H/C ratio, and the event ratio of this pair will have no contribution from this potential source of error.

2.4.2 H/Gd ratio

Neutrons are thermalized during their first 10μs of existence in the detector central volume. Thus for times longer than 10μs the delayed neutron capture events will exhibit an exponential time constant, τ, related to the average concentration of Gd in the detector module. The rate of capture, $\Gamma \equiv 1/\tau$, is given by:

$$\Gamma = \Gamma_{Gd} + \Gamma_H = [n_{Gd}\sigma_{Gd} + n_H\sigma_H]v \; . \tag{17}$$

The fraction of neutrons that capture on Gd rather than H is then

$$f_{Gd} = \frac{1}{1 + \Gamma_H/\Gamma_{Gd}} \tag{18}$$

and we would like to know this *relative* fraction between different detector modules to $\sim 0.1\%$. Thus we must measure the time constants τ for different detector modules to a *relative* precision of 0.2 μsec. The value of τ is expected to be about 30 μsec , so we need to measure it to about 0.5% relative precision. Such a measurement requires measuring about 30,000 neutron captures, which can be done in a few minutes with a neutron source. The CHOOZ experiment measured the (*absolute*) $\sim 30\mu$sec capture time to $\pm 0.5\mu$sec precision.

2.4.3 Energy cut efficiency

To reject uncorrelated backgrounds, CHOOZ employed a positron energy threshold of 1.3 MeV. This cut resulted in an estimated error of 0.8%. The improved design of the Daya Bay detector and shielding makes it possible to lower this threshold to below 1 MeV while keeping uncorrelated backgrounds as low as 0.1%. The threshold of visible energy of neutrino events is 1.022 MeV. Due to the finite energy resolution of $\sim 12\%$ at 1 MeV, the reconstructed energy will have a tail below 1 MeV. The systematic error associated with this cut efficiency is studied by Monte Carlo simulation. The tail of the simulated energy spectrum is shown in Fig. 2.3 with the full spectrum shown in the inset. For this simulation, 200 PMTs are used to measure the energy deposited in a 20-ton module. The energy resolution is $\sim$ 15% at 1 MeV. The inefficiencies are 0.32%, 0.37%, and 0.43% for cuts at 0.98 MeV, 1.0 MeV, and 1.02 MeV, respectively. Assuming the energy scale error is 2% at 1 MeV, this inefficiency variation will produce a 0.05% error in the detected antineutrino rate.

Another issue is the neutron detection efficiency associated with the signal from capture of neutrons on Gd in the central detector volume. An energy threshold of about 6 MeV will be employed to select these delayed events, and the efficiency of this criterion may vary between detector modules depending upon the detailed response of the module. However, this can be calibrated through the use of radioactive sources (see Chapter 8) and spallation neutron captures. The KamLAND detector gain is routinely (every 2 weeks) monitored with sources, and a relative long-term gain drift of $\sim 1\%$ is readily monitored with a precision of 0.05%. According to our Monte Carlo simulations, a 2% energy uncertainty at 6 MeV results in a 0.5% uncertainty in the neutron detection efficiency. We intend to calibrate the detector modules with a precision comparable to the KamLAND experience. This would enable us to achieve an improved neutron detection efficiency uncertainty of $\sim 0.013\%$.

2.4.4 Position and time cuts

Due to the design of the detector modules, the event rate is measured without resort to reconstruction of the event location. Therefore the error in the event rate is related to the physical parameters of the central volume. We do not anticipate employing cuts on reconstructed position to select events.

However, the time correlation of the prompt (positron) event and the delayed (neutron) event is a critical aspect of the event signature. Matching the time delays of the start and end times of this time window between detector modules is crucial to reducing systematic *uncertainties* associated with this aspect of the antineutrino signal. If the starting time ($\sim 0.3\mu$sec) and ending time ($\sim 200\mu$sec)of the delayed event window is determined to ~ 10 nsec precision, the resulting error associated with the lost event fraction is

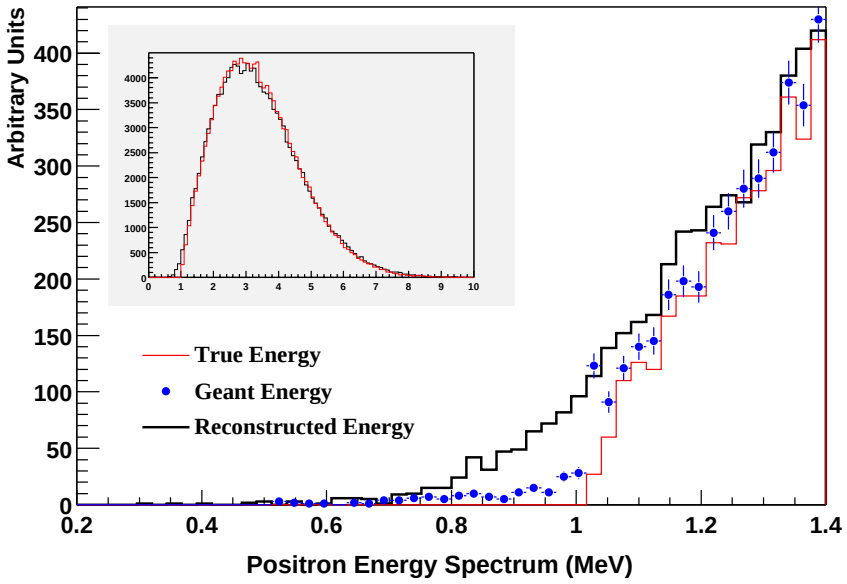

Fig. 2.3. Spectra of prompt energy for true energy, simulated energy (Geant Energy), and reconstructed energy at around 1 MeV. The full spectrum is shown in the inset, where the red line corresponds to the true energy and the black one corresponds to the reconstructed energy.

$\sim 0.03\%$. We will insure that this timing is equivalent for different detector modules by slaving all detector electronics to one master clock. We estimate that with due care, the relative neutron efficiency for different modules due to timing is known to $\sim 0.03\%$.

2.4.5 Neutron multiplicity

CHOOZ required a cut on the neutron multiplicity to eliminate events where it appeared that there were 2 neutron captures following the positron signal. These multiple neutron events are due to muon-induced spallation neutrons, and will be reduced to a much lower level by the increased overburden available at the Daya Bay site. For the near site at 500 m baseline, the muon rate relative to the signal rate will be more than a factor 9 lower than for the CHOOZ site. Therefore, events with multiple neutron signals will be reduced by this factor relative to CHOOZ, and should present a much smaller problem for the Daya Bay site.

2.4.6 Trigger

The trigger efficiency will be measured using studies with pulsed light sources in the detector. Through a series of careful measurements we should be able to measure the trigger efficiency of each detector system to high precision, 0.01%. (KamLAND has used this method to determine 99.8% absolute trigger efficiency[21].)

2.4.7 Live time

The detector live time can be measured accurately by counting a 100 MHz clock using the detector electronics, and normalizing to the number of clock ticks in a second (as defined by a GPS receiver signal). The uncertainty associated with this procedure should be extremely small, and certainly negligible relative to the other systematic *uncertainties*. For example, SNO measured the relative live times for their day/night analysis with a relative fractional uncertainty of 5×10^{-7}.

2.5 Cross-calibration and Swapping of Detectors

2.5.1 Detector Swapping

The connection of the two near detector halls and the far hall by horizontal tunnels provides the Daya Bay experiment with the unique and important option of swapping the detectors between the locations. This will enable the further reduction of detector-related systematic *uncertainties* in the measurement of the ratio of neutrino fluxes at the near and far locations.

The swapping concept is easy to demonstrate for a simple scenario with a single neutrino source and only 2 detectors deployed at 2 locations, near and far. The desired measurement is the ratio of event rates at the near and far locations: N/F. With detector #1 (efficiency ϵ_1) at the near location and detector #2 (efficiency ϵ_2)at the far location we would measure

$$\frac{N_1}{F_2} = \left(\frac{\epsilon_1}{\epsilon_2}\right)\frac{N}{F}\,. \tag{19}$$

By swapping the two detectors and making another measurement, we can measure

$$\frac{N_2}{F_1} = \left(\frac{\epsilon_2}{\epsilon_1}\right)\frac{N}{F}\,, \tag{20}$$

where we have assumed that the detector properties (e.g., efficiencies) do not change when the detector is relocated. We can now combine these two measurements to obtain a value of N/F that is, to first order, independent of the detector efficiencies:

$$\frac{1}{2}\left(\frac{N_1}{F_2} + \frac{N_2}{F_1}\right) = \frac{N}{F}\left(1 + \frac{\delta^2}{2}\right) \tag{21}$$

where we have defined

$$\delta \equiv \frac{\epsilon_2}{\epsilon_1} - 1\,. \tag{22}$$

Note that even if the detector efficiencies are different by as much as 1%, we can determine N/F to a fractional precision better than 10^{-4}.

The layout of the Daya Bay experiment involves 2 near sites with 2 detectors each, and a far site with 4 detectors. The simplest plan is to designate the eight detectors as 4 pairs: (1,2), (3,4), (5,6), (7,8). Using 4 running periods (designated I, II, III, IV, separated by three detector swapping events) we can arrange for each detector to be located at the far site half the time and a near site half the time by swapping 2 pairs between running periods, as shown in Table 2.3. Ratios of event rates can be combined in a fashion analogous to the above discussion to provide cancelation of detector-related systematic *uncertainties* and also reactor power systematic *uncertainties*. Careful calibration of the detectors following each swap will be necessary to insure that each detector's performance does not change significantly due to relocation.

Run Period	Near(DB)	Near(LA)	Far
I	1,3	5,7	2,4,6,8
II	2,3	6,7	1,4,5,8
III	2,4	6,8	1,3,5,7
IV	1,4	5,8	2,3,6,7

Table 2.3. Swapping scheme with 4 running periods. The detectors (labelled 1-8) are deployed at the Near(DB), Near(LA), and Far sites during each period as indicated in this table.

2.5.2 Detector Cross-calibration

Another important feature of the design of the Daya Bay experiment is the presence of two detector modules at each near site. During a single running period (I, II, III, or IV) each near detector module will measure the neutrino rate with 0.23% statistical precision. If the systematic *uncertainties* are smaller than this, the two detectors at the near site should measure the same rate, giving a detector asymmetry of $0 \pm 0.34\%$ (statistical error only). Combining all the detector pairs in all 4 running periods will yield an asymmetry of $0 \pm 0.04\%$ (statistical error only). These asymmetries are an important check that the detector-related systematic *uncertainties* are under control. In addition, this analysis can provide information on the the degree to which the detector-related systematic *uncertainties* are correlated or uncorrelated so that we know how to handle them in the full analysis including the far site.

Finally, the near detector data can provide important information on the reactor power measurements. We will measure the ratio

$$R_{\rm near} = \frac{S_{DB}}{S_{LA}} \tag{23}$$

where S_{DB} (S_{LA}) is the detector signal (normalized to the reactor power) for the Daya Bay (Ling Ao) near site. If the reactor powers are correct (and the detector systematic *uncertainties* are under control) then we expect $R_{\rm near} = 1.0 \pm 0.24\% \pm 0.51\%$, where the first error is statistical (only 1 of the 4 running periods) and the second error is the detector (baseline) systematic error. Note that these *uncertainties* are small relative to the expected 2% uncorrelated reactor power uncertainty, so measurement of $R_{\rm near}$ will provide an important check (and even perhaps additional information) on the reactor powers. Furthermore, studies of the measured neutrino spectra in the different near detectors during different parts of the reactor fuel cycle can help provide constraints on the fuel cycle effects on the spectrum.

2.6 Backgrounds

In the Daya Bay experiment, the signal events (inverse beta decay reactions) have a distinct signature of two time-ordered signals: a prompt positron signal followed by a delayed neutron-capture signal. Backgrounds can be classified into two categories: correlated and uncorrelated backgrounds. If a background event is triggered by two signals that come from the same source, such as those induced by the same cosmic muon, it is a correlated background event. On the other hand, if the two signals come from different sources but satisfy the trigger requirements by chance, the event is an uncorrelated background.

There are three important sources of backgrounds in the Daya Bay experiment: fast neutrons, ^{8}He/ ^{9}Li, and natural radioactivity. A fast neutron produced by cosmic muons in the surrounding rock or the detector can produce a signal mimicking the inverse beta decay reaction in the detector: the recoil proton generates the prompt signal and the capture of the thermalized neutron provides the delayed signal. The ^{8}He/ ^{9}Li isotopes produced by cosmic muons have substantial beta-neutron decay branching fractions, 16% for ^{8}He and 49.5% for ^{9}Li. The beta energy of the beta-neutron cascade overlaps the positron signal of neutrino events, simulating the prompt signal, and the neutron emission forms the delayed signal. Fast neutrons and ^{8}He/ ^{9}Li isotopes create correlated backgrounds since both the prompt and delayed signals are from the same single parent muon. Some neutrons produced by cosmic muons are captured in the detector without proton recoil energy. A single neutron capture signal has some probability to fall accidentally within the time window of a preceding signal due to natural radioactivity in the detector, producing an accidental background. In this case, the prompt and delayed signals are from different sources, forming an uncorrelated background.

All three major backgrounds are related to cosmic muons. Locating the detectors at sites with adequate overburden is the only way to reduce the muon flux and the associated background to a tolerable level. The overburden requirements for the near and far sites are quite different because the signal rates differ by more than a factor of 10. Supplemented with a good muon identifier outside the detector, we can tag the muons going through or near the detector modules and reject backgrounds efficiently.

In this section, we describe our background studies and our strategies for background management. We conclude that the background-to-signal ratio will be around 0.5% at the near sites and around 0.2% at the

far site, and that the major sources of background can be quantitatively studied *in-situ*.

2.6.1 Cosmic muons at underground laboratories

The most effective and reliable approach to minimize the backgrounds in the Daya Bay experiment is to have sufficient amount of overburden over the detectors. The Daya Bay site is particularly attractive because it is located next to a 700-m high mountain. The overburden is a major factor in determining the optimal detector sites. The location of detector sites has been optimized by using a global χ^2 analysis described in section 2.7.1.

Detailed simulation of the cosmogenic background requires accurate information of the mountain profile and rock composition. Fig. 2.4 shows the mountain profile converted from a digitized 1:5000 topographic map. The horizontal tunnel and detector sites are designed to be about 10 m below sea level. Several rock samples at different locations of the Daya Bay site were analyzed by two independent groups. The measured rock density ranges from 2.58 to 2.68 g/cm^3. We assume an uniform rock density of 2.60 g/cm^3 in the present background simulation.

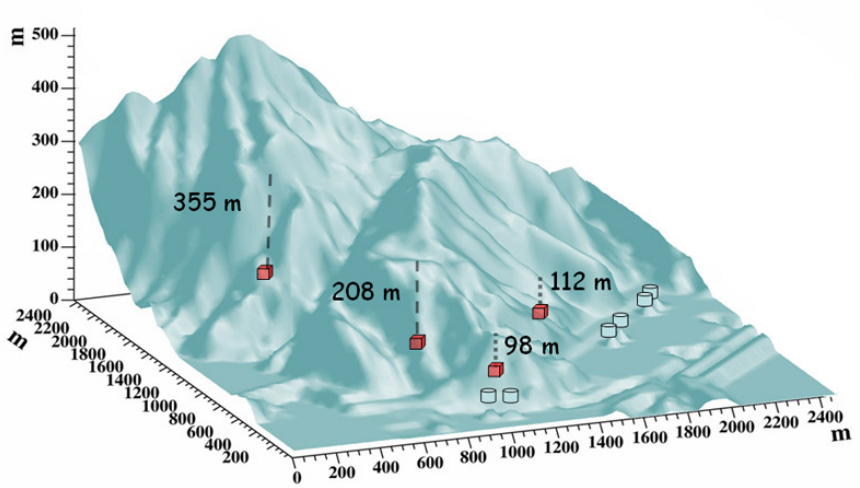

Fig. 2.4. Three dimensional profile of Pai Ya Mountain generated from a 1:5000 topographic map of the Daya Bay area.

The standard Gaisser formula is known to poorly describe the muon flux at large zenith angle and at low energies. This is relevant for the Daya Bay experiment since the overburden at the near sites is only $\sim$ 100 m. We modified the Gaisser formula[2] to describe the muon flux at the sea level. The comparison of the modified formula with data is shown in Fig. 2.5, where the calculations with the standard Gaisser formula are also shown. At muon energies of several tens of GeV, the standard Gaisser formula has large discrepancies with data while the modified formula agrees with data in the whole energy range.

Using the mountain profile data, the cosmic muons are transported from the atmosphere to the underground detector sites using the MUSIC package[1]. Simulation results are shown in Table 2.4 for the optimal detector sites. The muon energy spectra at the detector sites are shown in Fig. 2.6. The four curves from upper to lower corresponds to the Daya Bay near site, the Ling Ao near site, the mid site and the far site, respectively.

2.6.2 Simulation of neutron backgrounds

The neutron production rates will depend upon the cosmic muon flux and average energy at the detector. However, the neutron backgrounds in the detector also depend on the local detector shielding. The neutrino detectors will be shielded by at least 2 meters of water. The veto water will be used as a Cerenkov detector to detect muons. Thus neutrons produced by muons in the detector module or the water shield will be identified by the muon signal in the water veto detector. In addition, neutrons created by muons in the surrounding

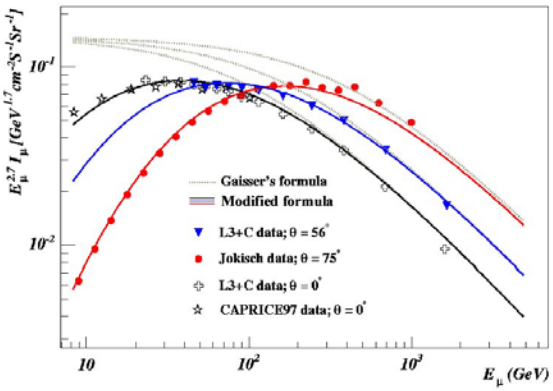

Fig. 2.5. Comparison of the modified formula (solid lines) with data. Calculations with the standard Gaisser's formula are shown in dashed lines. The data are taken from Ref.[4,5].

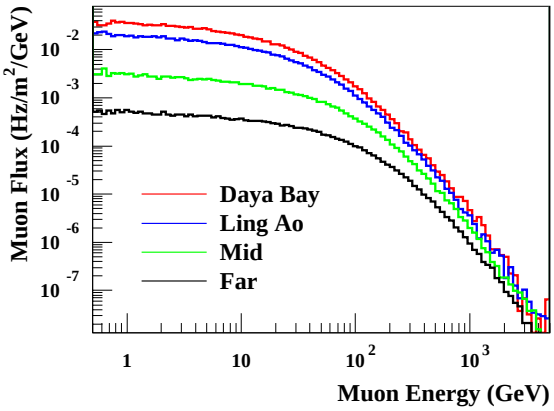

Fig. 2.6. Muon flux as a function of the energy of the surviving muons. The four curves from upper to lower corresponds to the Daya Bay near site, the Ling Ao near site, the mid site and the far site, respectively.

	DYB site	LA site	Mid site	Far site
Vertical overburden (m)	98	112	208	355
Muon Flux (Hz/m^2)	1.16	0.73	0.17	0.041
Muon Mean Energy (GeV)	55	60	97	138

Table 2.4. Vertical overburden of the detector sites and the corresponding muon flux and mean energy.

rock will be effectively attenuated by the 2 m water shield. Together with another muon tracker outside the veto water, the combined muon tag efficiency is designed to be 99.5%, with an uncertainty smaller than 0.25%.

With the detailed muon flux and mean energy at each detector site, the neutron yield, energy spectrum, and angular distribution can be estimated with an empirical formula[6] which has been tested against experimental data whenever available. A full Monte Carlo simulation has been carried out to propagate the primary neutrons produced by muons in the surrounding rocks and the water buffer to the detector. The primary neutrons are associated with their parent muons in the simulation so that we know if they can be tagged by the veto detector. All neutrons produced in the water buffer will be tagged with an efficiency of 99.5%, since their parent muons must pass through the muon systems. About 30% of the neutrons produced in the surrounding rocks cannot be tagged. The neutrons produced in the rocks, however, have to survive at least 2 meters of water. The neutron background after veto rejection is the sum of the untagged events and 0.5% of the tagged events.

Some energetic neutrons will produce tertiary particles, including neutrons. For those events that have energy deposited in the liquid scintillator, quite a lot of them have a complex time structure due to multiple neutron scattering and captures. These events are split into sub-events in 50 ns time bins. We are interested in two kinds of events. The first kind has two sub-events. The first sub-event has deposited energy in the range of 1 to 8 MeV, followed by a sub-event with deposited energy in the range of 6 to 12 MeV in a time window of 1 to 200μs. These events, called fast neutron events, can mimic the antineutrino signal as correlated backgrounds. The energy spectrum of the prompt signal of the fast neutron events, e.g. at the far

site, is shown in Fig. 2.7 up to 50 MeV. The other kind of events has only one sub-event with deposited energy in range of 6 to 12 MeV. These events, when combined with the natural radioactivity events, can provide the delayed signal to form the uncorrelated backgrounds. We call them single neutron events. The neutron simulation results are listed in Table 2.5.

		DYB site	LA site	far site
fast neutron	vetoed	57.8	45.6	3.8
(/day/module)	not vetoed	0.83	0.64	0.08
single neutron	vetoed	1365	1070	94.7
(/day/module)	not vetoed	27.2	21.0	2.1

Table 2.5. Neutron rates in a 20-ton module at the Daya Bay sites. The rows labelled "vetoed" refer to the case where the parent muon track traversed the veto detectors, and thus it could be tagged. Rows labelled "not vetoed" refer to the case where the muon track did not traverse the veto detectors. (numbers to be updated.)

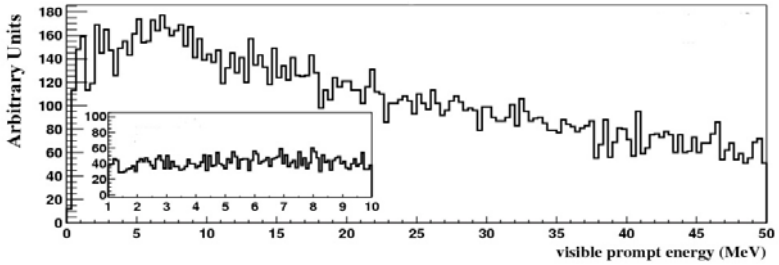

Fig. 2.7. The prompt energy spectrum of fast neutron backgrounds at the Daya Bay far detector. The inset is an expanded view of the spectrum from 1 to 10 MeV.

The rate and energy spectrum of the fast neutron backgrounds can be studied with the tagged sample, which is 200 times larger than the untagged one.

2.6.3 Cosmogenic isotopes

Cosmic muons, even if they are tagged by the muon identifier, can produce radioactive isotopes in the detector scintillator which decay by emitting both a beta and a neutron (β-neutron emission isotopes). Some of these so-called cosmogenic radioactive isotopes live long enough such that their decay cannot be reliably associated with the last vetoed muon. Among them, ^{8}He and ^{9}Li with half-lives of 0.12 s and 0.18 s, respectively, constitute the most serious correlated background sources. The production cross section of these two isotopes has been measured with muons at an energy of 190 GeV at CERN[10]. Their combined cross section is $\sigma(^{9}\mathrm{Li} + ^{8}\mathrm{He}) = (2.12 \pm 0.35)\mu\mathrm{barn}$. Since their lifetimes are so close, it is hard to get their individual cross sections. About 16% of ^{8}He and 49.5% of ^{9}Li will decay by β-neutron emission. Using the muon flux and mean energy given in last section at the detector sites and an energy dependence of the cross section, $\sigma_{\mathrm{tot}}(E_\mu) \propto E_\mu^\alpha$, with $\alpha = 0.74$, the ^{8}He+^{9}Li backgrounds are estimated to be

	DYB site	LA site	Far site
(^{8}He+^{9}Li)/day/module	3.7	2.5	0.26

The KamLAND experiment measures this ^{9}Li/ ^{8}He background very well by fitting the time since last muon. The muon rate is 0.3 Hz in the active volume of KamLAND detector. The mean time interval of

successive muons is 5 seconds, much longer than the lifetimes of ^{9}Li/ ^{8}He. For the Daya Bay experiment, the target volume of a 20 ton detector module has a cross section around 10 m^2, thus the muon rate is around 10 Hz at the near sites, resulting in a mean time interval of successive muons shorter than the lifetimes of ^{9}Li/^{8}He. With a modified fitting algorithm, we find that it is still feasible to measure the isotope background *in-situ*.

From the decay time and β-energy spectra fit, the contribution of ^{8}He relative to that of ^{9}Li was determined by KamLAND to be less than 15% at 90% confidence level[11]. Furthermore, the ^{8}He contribution can be identified by tagging the double cascade ^{8}He $\rightarrow^8$Li $\rightarrow^8$Be. So we assume that all isotope backgrounds are ^{9}Li. They can be determined with a maximum likelihood fitting even at 10 Hz muon rate, by taking all contributions from the preceding muons into account. The resolution of the background-to-signal ratio can be determined to be[12]

$$\sigma_b = \frac{1}{\sqrt{N}} \cdot \sqrt{(1+\tau R_\mu)^2 - 1}\,, \tag{24}$$

where N is the total number of neutrino candidates, τ is the lifetime of ^{9}Li, and R_μ is the muon rate in the target volume of detector. The resolution is insensitive to the ^{9}Li level since the statistical fluctuation of neutrino events dominates the uncertainty. The background-to-signal ratio of ^{9}Li background can be measured to $\sim 0.3\%$ with two 20-ton modules at the near sites of the Daya Bay experiment and $\sim 0.1\%$ at the far site with four 20-ton modules, with the data sample of three years of running. The fitting uses time information only. Inclusion of energy and vertex information could further improve the precision.

A Monte Carlo has been carried out to check the fitting algorithm. The background-to-signal ratio is fixed at 1%. The total number of neutrino candidates is 2.5×10^5, corresponding to the far site statistical error, 0.2%. Fig. 2.8 shows the fitting results as a function of muon rate. The data sample generation and fitting were performed 400 times for each point to get the fitting precision. In Fig. 2.9 the fitting precision is compared to the analytic formula Eq. 24 with the same Monte Carlo samples. The Monte Carlo results for minimizing χ^2, the maximum likelihood fit, and the simple analytical estimation are in excellent agreement.

KamLAND also found that most (perhaps all) ^{8}He/ ^{9}Li background are produced by showering muons[11]. A 2-second veto of the whole detector is applied at KamLAND to reject these backgrounds. Roughly 3% of cosmic muons shower in the detector. It is not feasible for Daya Bay to apply a 2-second veto since the dead time of the near detector would be more than 50%. However, if the Daya Bay detector is vetoed for 0.5 s after a showering muon, about 85% isotope backgrounds caused by shower muons can be rejected. Approximately 30% of the ^{8}He/ ^{9}Li background will remain: $\sim 15\%$ from non-showering muons and $\sim 15\%$ from showering muons. Although additional *uncertainties* may be introduced due to the uncertainties in the relative contributions from showering and non-showering muons and the uncertainties arising from the additional cuts (e.g., increased dead time), this rejection method can cross check the fitting method and firmly determine the background-to-signal ratio to 0.3% at the near sites and to 0.1% at the far site.

2.6.4 Radioactivity

Natural radioactivity and the single neutron events induced by cosmic muons may occur within a given time window accidentally to form an uncorrelated background. The coincidence rate is given by $R_\gamma R_n \tau$, where R_γ is the rate of natural radioactivity events, R_n is the rate of spallation neutron, and τ is the length of the time window. With the single neutron event rate given in previous section, the radioactivity should be controlled to 50 Hz to limit the accidental backgrounds $< 0.1\%$. The accidental backgrounds can be well determined *in-situ* by measurement of the individual single rates from radioactivity and the single neutrons. The energy spectrum can be also well determined.

Past experiments suppressed uncorrelated backgrounds with a combination of using carefully selected construction materials, self-shielding, and using absorbers that have large neutron capture cross section. However, additional care is necessary to lower the detector energy threshold much below 1 MeV. A higher threshold will introduce a systematic error in the efficiency of detecting the positron. In the following, the singles rate is the radioactivity of > 1 MeV visible energy in detector.

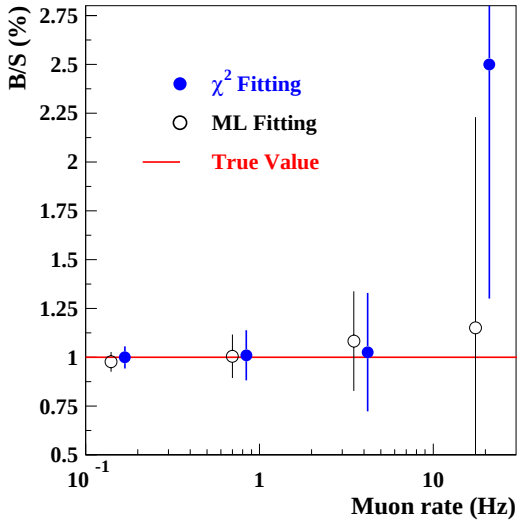

Fig. 2.8. Fitting results as a function of the muon rate. The error bars show the precision of the fitting. The χ^2 fitting uses the same muon rate as ML fitting but shown on the right of it.

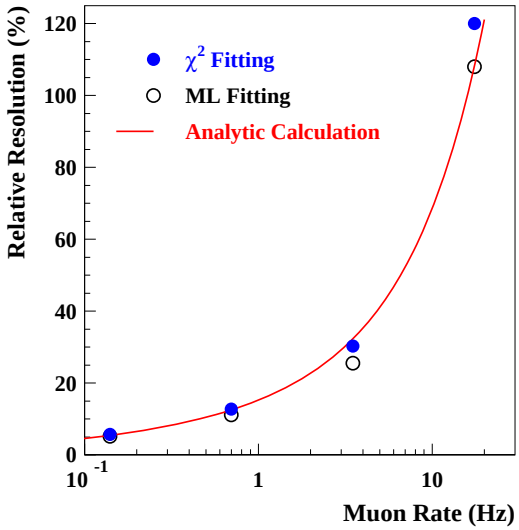

Fig. 2.9. The fitting precision as a function of the muon rate, comparing with the analytic estimation of Eq. 24. The y-axis shows the relative resolution of the background-to-signal ratio.

Radioactive background can come from a variety of sources:

- U/Th/K in the rocks around the detector hall.
- U/Th/K in the veto water.
- ^{60}Co in the detector vessel and other supporting structures.
- U/Th/K in the PMT glass.
- U/Th/K in the scintillator.
- U/Th/K in materials used in the detector.
- Radon in air.
- Cosmic rays.

The radioactivity of the rock samples from the Daya Bay site have been measured by several independent groups. The concentration is $\sim$ 10 ppm for ^{238}U, $\sim$ 30 ppm for ^{232}Th, and $\sim$ 5 ppm for ^{40}K. The rock radioactivity has been studied with Monte Carlo. With the shielding of 2-meter veto water and 45 cm oil buffer, there are 5 Hz, 20 Hz, and 2 Hz singles rate of visible energy greater than 1 MeV at each center detector module, for U/Th/K respectively. The total rate is $\sim$ 27 Hz.

The geological environment and rock composition are very similar for Hong Kong and Daya Bay. The spectrum of the natural radioactivity of the rocks in the Aberdeen Tunnel in Hong Kong is shown in Fig. 2.10.

The veto water will be circulated and purified to achieve enough attenuation length for water Cerenkov light as well as low radioactivity. KamLAND veto water has 1 ppb ^{238}U, 1 ppb ^{232}Th, and also 1 ppb ^{40}K.

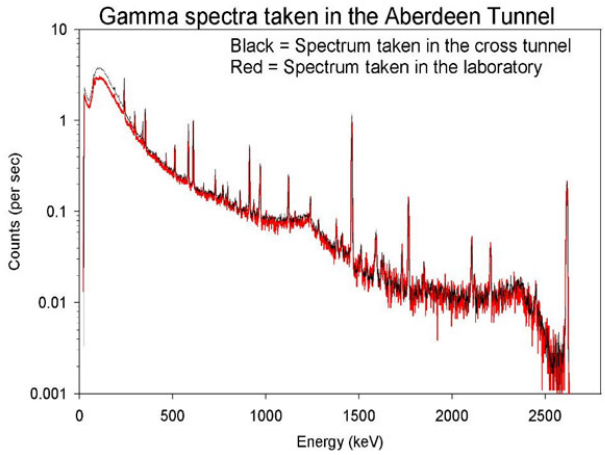

Fig. 2.10. Spectrum of natural radioactivity measured with a Ge crystal in the Hong Kong Aberdeen Tunnel.

Assuming the same concentration, the veto water will contribute 1.8 Hz, 0.4 Hz, and 6.3 Hz single rates from U/Th/K, respectively.

The ^{60}Co in stainless steel varies from batch to batch and should be measured before use as detector material, such as the outer vessel. Conservatively, assuming 1 pCi/kg ^{60}Co in the outer vessel, the single rates will be $\sim$ 6 Hz.

A potential PMT candidate is the Hamamatsu R5912 with low radioactivity glass. The concentrations of ^{238}U and ^{232}Th are both less than 40 ppb in the glass, and that of ^{40}K is 25 ppb. The Monte Carlo study shows that the single rate is 2.2 Hz, 1 Hz, 4.5 Hz for U/Th/K, respectively, with 20 cm oil buffer from the PMT surface to the liquid scintillator. The total rate from the PMT glass is 7.7 Hz.

Following the design experience of Borexino and Chooz, backgrounds from impurities in the detector materials can be reduced to the required levels. The U/Th/K concentration of $10^{-12} g/g$ in liquid scintillator will contribute only 0.8 Hz of background in a 20 ton module.

Radon is one of the radioactive daughters of ^{238}U, which can increase the background rate of the experiment. The Radon concentration in the experimental halls can be kept to an acceptable level by ventilation with fresh air from outside. Since the neutrino detector modules are immersed in 2-meter thick water buffer, it is expected that the radon contribution can be safely ignored for the water pool design.

The β decay of long lived radioactive isotopes produced by cosmic muons in the scintillator will contribute a couple of Hz at the near detector, and less than 0.1 Hz at the far detector. The rate of accidental coincidence induced by muon decay or muon capture is less than the muon rate. So they can be ignored too.

2.6.5 Background subtraction error

There are other sources of backgrounds, such as cosmogenic nuclei, stopped-muon decay, and muon capture. While they are important for a shallow site, our study shows that they can be safely ignored at Daya Bay.

Assuming 99.5% muon veto efficiency, the three major backgrounds are summarized below while the other sources are negligible. In our sensitivity study, the *uncertainties* were taken to be 100% for the accidental and fast neutron backgrounds. The ^{8}He/ ^{9}Li background can be measured to an uncertainty of 0.3% and 0.1% at the near and far sites, respectively.

The rates and energy spectra of all three major backgrounds can be measured *in-situ*. Thus the backgrounds at the Daya Bay experiment are well controlled. The simulated energy spectra of backgrounds are shown in Fig. 2.6.5. The background-to-signal ratios are taken at the far site. The oscillation signal is the

	DYB site	LA site	far site
Neutrino rate (/day/module)	930	760	90
Natural radiation (Hz)	<50	<50	<50
Single neutron (/day/module)	34	26	2.6
Accidental/Signal	<0.05%	<0.05%	<0.05%
Fast neutron/Signal	0.14%	0.1%	0.1%
^{8}He^{9}Li/Signal	0.3%	0.2%	0.2%

Table 2.6. Summary of backgrounds. The neutrino rate and single neutron rates has been applied an neutron detection efficiency of 78%.

difference of the expected neutrino signal without oscillation and the "observed" signal with oscillation if $\sin^2 2\theta_{13} = 0.01$.

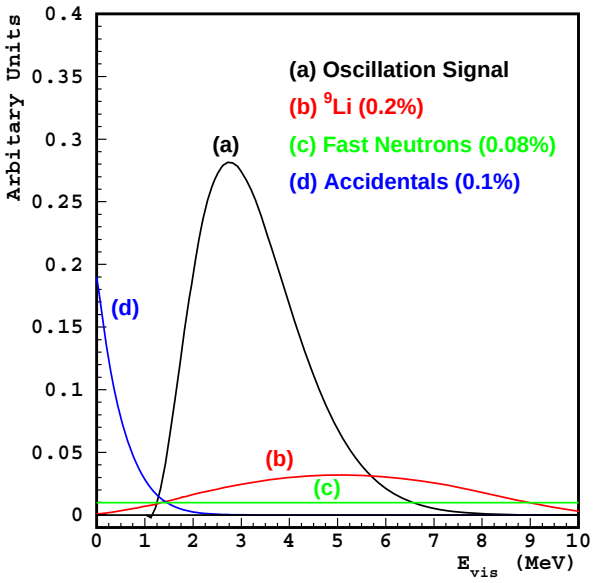

Fig. 2.11. Spectra of three major backgrounds for the Daya Bay experiment and their size relative to the oscillation signal.

2.7 Sensitivity

2.7.1 Global χ^2 analysis

If θ_{13} is non-zero, a rate deficit will be present at the far detector due to oscillation. At the same time, the energy spectra of neutrino events at the near and far detectors will be different because neutrinos of different energies oscillate at different frequencies. Both rate deficit and spectral distortion of neutrino signal will be explored in the final analysis to obtain maximum sensitivity. When the neutrino event statistics is low, say $<$ 400 ton·GW·y, the sensitivity is dominated by the rate deficit. For luminosities higher than 8000 ton·GW·y, the sensitivity is dominated by the spectral distortion[30]. The Daya Bay experiment will have $\sim$ 3000 ton·GW·y exposure in three years, where both rate deficit and shape distortion will be important to the analysis.

Many systematic *uncertainties* will contribute to the final sensitivity of the Daya Bay experiment, and

many of the *uncertainties* are correlated, which must be taken into account. A rigorous analysis of systematic *uncertainties* can be done by constructing a χ^2 function with pull terms, where the error correlations can be introduced naturally[28–31]:

$$\begin{aligned}\chi^2 &= \min_{\gamma} \sum_{A=1}^{3} \sum_{i=1}^{N_{bins}} \frac{\left[M_i^A - T_i^A\left(1+\alpha_c+\sum_r \omega_r^A \alpha_r + \beta_i + \varepsilon_D + \varepsilon_d^A\right) - \eta_f^A F_i^A - \eta_n^A N_i^A - \eta_s^A S_i^A\right]^2}{T_i^A + \sigma_{b2b}^2} \\ &+ \frac{\alpha_c^2}{\sigma_c^2} + \sum_r \frac{\alpha_r^2}{\sigma_r^2} + \sum_{i=1}^{N_{bins}} \frac{\beta_i^2}{\sigma_{\rm shp}^2} + \frac{\varepsilon_D^2}{\sigma_D^2} + \sum_{A=1}^{3}\left[\left(\frac{\varepsilon_d^A}{\sigma_d}\right)^2 + \left(\frac{\eta_f^A}{\sigma_f^A}\right)^2 + \left(\frac{\eta_n^A}{\sigma_n^A}\right)^2 + \left(\frac{\eta_s^A}{\sigma_s^A}\right)^2\right], \end{aligned} \tag{25}$$

where A sums over detectors, i sums over energy bins, and γ denotes the set of minimization parameters, $\gamma = \{\alpha_c, \alpha_r, \beta_i, \varepsilon_D, \varepsilon_d^A, \eta_f^A, \eta_n^A, \eta_s^A\}$. The γ_s are used to introduce different sources of systematic *uncertainties*. The standard deviations of the corresponding parameters are $\{\sigma_c, \sigma_r, \sigma_{\rm shp}, \sigma_D, \sigma_d, \sigma_f^A, \sigma_n^A, \sigma_s^A\}$. For each energy bin, there is a statistical error T_i^A and a bin-to-bin systematic error σ_{b2b}. For each point in the oscillation space, the χ^2 function has to be minimized with respect to the parameter γ_s.

Assuming each error can be approximated by a Gaussian, this form of χ^2 can be proven to be strictly equivalent to the more familiar covariance matrix form $\chi^2 = (M-T)^T V^{-1}(M-T)$, where V is the covariance matrix of $(M-T)$ with systematic *uncertainties* included properly[28]. The systematic *uncertainties* are described one by one in the following.

- Reactor-related correlated error $\sigma_c \approx 2\%$. This fully correlated error will be cancelled by the near-far relative measurement and has almost no impact on the sensitivity.
- Reactor-related uncorrelated error $\sigma_r \approx 2\%$. After minimization, it contributes $\sim 0.1\%$ to the normalization of neutrino rate, as described in sec. 2.1.
- Shape error $\sigma_{\rm shp} \approx 2\%$: Shape error is the uncertainty on neutrino energy spectra calculated from reactor information. This error is uncorrelated between different energy bins but correlated between different detectors. Since we have enough statistics at near detector to measure neutrino energy spectrum to much better than 2%, in addition to this calculation, it has little impact for Daya Bay sensitivity.
- Detector-related correlated error $\sigma_D \approx 2\%$. Some detection *uncertainties* are common to all detectors, such as H/Gd ratio, H/C ratio, neutron capture time on Gd, and edge effect, assuming we use the same batch of liquid scintillator and identical detectors. Based on Chooz's experience, σ_D is (1 - 2)%. Like other fully correlated *uncertainties*, it has almost no impact on sensitivity.
- Detector-related uncorrelated error $\sigma_d \approx 0.2\%$. Detector-related uncorrelated *uncertainties* include the mass of active volume, live time, etc., which do not cancel out with near-far measurement. It is estimated to be 0.36% for a single detector module. However, with detector swapping between the near and far sites, most will cancel too. Those can not cancel are mainly related with the *energy-scale* uncertainties, such as positron and neutron detection efficiency. They are estimated to be $\sim 0.2\%$.
- Background rate error σ_f^A, σ_n^A, and σ_s^A, labelling the rate error of fast neutron, accidental backgrounds, and isotopes. They are listed in table 2.6.
- Bin-to-bin error σ_{b2b}: Bin-to-bin error is systematic error that is uncorrelated between energy bins and uncorrelated between different detector modules. The bin-to-bin *uncertainties* normally arise from the different energy scale at different energies and uncertainties of background energy spectra during background subtraction. Up to now, the only reactor neutrino experiment that performed spectral analysis with large statistics is Bugey, which has bin-to-bin error of order of 0.5%[25,26]. With better designed detectors and much less background, we should have much smaller bin-to-bin *uncertainties* than Bugey. The bin-to-bin error can be studied by comparing the spectra of two detector modules at the same site. We will use 0.5% in the sensitivity analysis.

There are other *uncertainties* not included in the χ^2 function. 1) Due to the energy resolution, the spectra are distorted. However, the energy bins used for sensitivity analysis ($\sim$ 30 bins) is $2 \sim 6$ times larger than the energy resolution, and the distortion happens at all detectors in the same way. It has almost no impact on the final sensitivity. 2) Detector energy scale error has significant impact on detection *uncertainties* (neutron efficiency and positron efficiency). It is taken into account in σ_d. At the same time, an energy scale error will shift the whole spectrum, thus directly impacting the analysis, especially on the best fit values. However, this shift is not a distortion, and cannot mimic oscillation. It has very little impact on sensitivity computations. 3) Current knowledge on θ_{12} and Δm_{21} has around 10% *uncertainties*. Although the net oscillation effect at Daya Bay baseline is related to θ_{13} only, the subtraction of θ_{12} oscillation effects might bring *uncertainties*.

We have studied the above three sources *of uncertainty* and found none of them having a significant impact on the sensitivity of the Daya Bay experiment. For simplicity, they are ignored in our χ^2 analysis of sensitivity.

2.7.2 θ_{13} sensitivity

Fig. 2.12 shows the sensitivity contours in the $\sin^2 2\theta_{13}$ versus Δm^2_{31} plane for three years of data, using the global χ^2 analysis. The green area covers the 90% confidence region of Δm^2_{31} determined by solar neutrino experiments. Taking a design with four 20-ton modules at the far site and two 20-ton modules at each near site, the statistical *uncertainty* is around 0.2%. The sensitivity of the Daya Bay experiment with this design can achieve the challenging goal of 0.01 with 90% confidence level in almost the whole range of Δm^2_{31}.

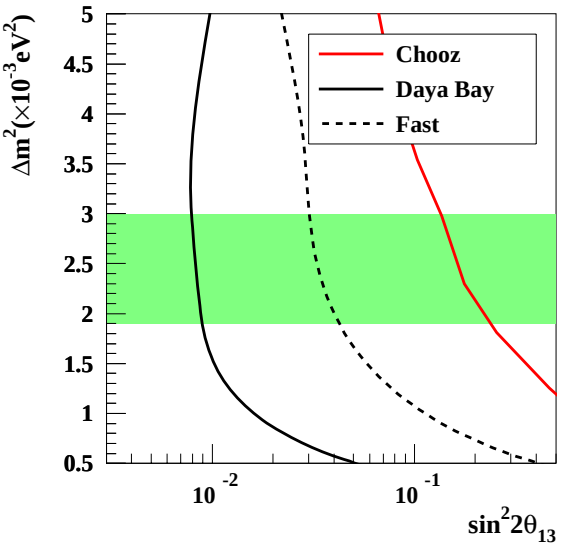

Fig. 2.12. Expected $\sin^2 2\theta_{13}$ sensitivity at 90% C.L. with 3 years of data, as shown in solid black line. The dashed line shows the sensitivity of the fast measurement with the DYB near site and the mid site only. The red line shows current upper limit measured by Chooz.

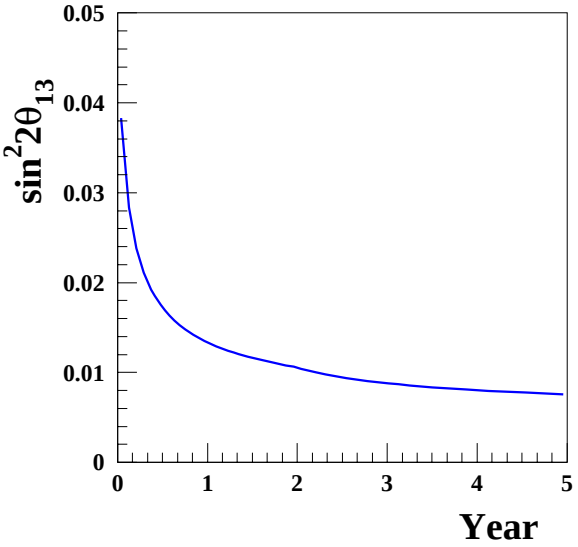

Fig. 2.13. Expected $\sin^2 2\theta_{13}$ sensitivity at 90% C.L. versus year of data taking of the full measurement, with two near sites and one far site. The Δm^2 is taken to be 2.5×10^{-3} eV^2.

Fig. 2.13 shows the sensitivity versus time of data taking. After one year of data taking, $\sin^2 2\theta_{13}$ sensitivity will reach 0.014 (1.4%) at 90% confidence level.

The tunnel of the Daya Bay experiment will have a total length around 3 km. The tunnelling will take 1 $\sim$ 2 years. To accelerate the experiment, the first completed experimental hall, the Daya Bay near hall, can be used for detector commissioning. Furthermore, it is possible to conduct a fast experiment with only two detector sites, the Daya Bay near site and the mid site. For this fast experiment, the "far detector", which is located at the mid hall, is not at the optimal baseline. At the same time, the reactor-related *uncertainty* would be 0.7%, very large compared with that of the full experiment. However, the sensitivity is still much better than the current best limit of $\sin^2 2\theta_{13}$. It is noteworthy that the improvement comes from better background shielding and improved experiment design. The sensitivity of the fast experiment for one year data taking is shown in Fig. 2.12 in dashed line. With one year's data, the sensitivity is around 0.03 for $\Delta m^{\,2} = 2.5 \times 10^{-3}$ eV^2, compared with the current best limit of 0.17 from the Chooz experiment.

2.7.3 Direct measurement of Δm^2_{31}

1. P. Antonioli *et al.,* Astro. Phys. **7**, 357 (1997).
2. T. Gaisser, *Cosmic Rays and Particle Physics* (Cambridge University Press, 1991).
3. Y. Muraki *et al.,* Phys. Rev. D **28**, 40 (1983).
4. J. Kremer *et al.,* Phys. Rev. Lett. **83**, 4241 (1999)
5. H. Jokisch *et al.,* Phys. Rev. D **19**, 1368 (1979).
6. Y. F. Wang *et al.,* Phys. Rev. D **64**, 013012 (2001).
7. M. Apollonio *et al.,* Phys. Lett. **420B**, 397 (1998); Phys. Lett. **466B**, 415 (1999); Euro. Phys. J. C **27**, 331 (2003).
8. M. Ambrosio *et al.* (The MACRO Collaboration), Phys. Rev. D **52**, 3793 (1995); M. Aglietta *et al.* (LVD Collaboration), Phys. Rev. D **60**, 112001 (1999); Ch. Berger *et al.* (Frejus Collaboration), Phys. Rev. D **40**, 2163 (1989).
9. *Atomic Data and Nuclear Data Tables*, Vol. **78**, No. 2 (July, 2001).
10. T. Hagner *et al.,* Astro. Phys. **14**, 33 (2000).
11. T. Araki *et al.* (KamLAND Collaboration), Phys. Rev. Lett. **94**, 081801 (2005).
12. L. Wen *et al.*, Nucl. Instr. and Meth. A **564**, 471 (2006).
13. K. S. McKinny, *A Search for Astrophysical Electron Anti-neutrinos at KamLAND*, Ph. D thesis, University of Alabama.
14. F. Ardellier *et al.*, *Double-CHOOZ: a Search for the Mixing Angle* θ_{13} (June 20, 2006), hep-ex/0606025.
15. J. A. Rice, *Mathematical Statistics and Data Analysis*, 2nd ed. (Wadsworth Publishing Co., Inc., 1993).
16. F. Ashton, H. J. Edwards, and G. N. Kelly, J. Phys. A **4**, 352 (1971).
17. K. Anderson, *et al., A New Nuclear Reactor Neutrino Experiment to Measure* θ_{13} (Feb. 26, 2004), hep-ex/0402041.
18. Y. F. Wang *et al.,* Phys. Rev. D **62**, 013012 (2000).
19. A. Piepke *et al.,* Nucl. Instr. and Meth. A **432**, 392 (1999); F. Boehm *et al.,* Phys. Rev. D **62**, 072002 (2000).
20. F. Boehm *et al.,* Phys. Rev. D **64**, 112001 (2001); Phys. Rev. D **62**, 072002 (2000); Phys. Rev. D **62**, 092005 (2000).
21. K. Eguchi *et al.,* Phys. Rev. Lett. **90**, 021802 (2003).
22. L. A. Mikaelyan and V. V. Sinev, Phys. Atom. Nucl. **63**, 1002 (2000); L. A. Mikaelyan, Nucl. Phys. Proc. Suppl. **91**, 120 (2001); L. A. Mikaelyan, Phys. Atom. Nucl. **65**, 1173 (2002).
23. F. Suekane, *The systematic error induced from the baseline differences in Kashiwazaki-Kariwa* $\sin^2 2\theta_{13}$ *experiment: A conceptual description* (unpublished).
24. H. Kwon *et al.,,* Phys. Rev. D **24**, 1097 (1981).
25. Y. Declais *et al.,* Phys. Lett. **B338**, 383 (1994); B. Ackar *et al.,* Nucl. Phys. **B434**, 503 (1995); B. Ackar *et al.,* Phys. Lett. **B374**, 243 (1996).
26. H. Sugiyama and O. Yasuda, *A formula for the sensitivity to* $\sin^2 2\theta_{13}$ *in reactor experiments with a spectral analysis* (Aug. 8, 2005), hep-ph/0508090.
27. P. Vogel *et al.*, Phys. Rev. C **24**, 1543 (1981); K. Schreckenbach *et al.,* Phys. Lett. **B160**, 325 (1985); A. A. Hahn *et al.*, Phys. Lett. **B218**, 365 (1989).
28. D. Stump *et al.*, Phys. Rev. D **65**, 014012 (2001).

29. Y. Fukuda *et al.*, Phys. Rev. Lett. **81**, 1562 (1998); Y. Ashie *et al.*, Phys. Rev. D **71**, 112005 (2005).
30. P. Huber, M. Lindner, T. Schwetz, and W. Winter, Nucl. Phys. **B665**, 487 (2003); Nucl. Phys. **B645**, 3 (2002).
31. H. Minakata *et al.*, Phys. Rev. D **68**, 033017 (2003); H. Minakata and H. Sugiyama, Phys. Lett. **B580**, 216 (2004).